Performance maps for an air-cooled air conditioning system as a preliminary instrument for the diagnosis of evaporator fouling

P. Catrini[1], A. Piacentino[1], J. E. Braun[2], A. Patil[2], A. L. Hjortland[2]

[1] Dpt. of Energy, ICT and Mathematical Models (DEIM), University of Palermo, Viale delle Scienze, 90128, Palermo, Italy
[2] Ray W. Herrick Laboratories, School of Mechanical Engineering, Purdue University, 177 S. Russell Street, West Lafayette, IN 47907-2099, USA

E-mail:catrinipietro@gmail.com

Abstract. During the past few decades, there has been increased interest in the development of automated approaches for detecting and diagnosing faults in air conditioning systems. Among them, thermoeconomic diagnosis is a technique which involves the use of exergy analysis. As a first step towards improving its performance, this work is focused on the thermodynamic and exergy analysis of a direct expansion air conditioning system used in small commercial building applications. The analysis was carried out by means of experimental activities on a 17.5 kW rooftop unit installed at the Herrick Laboratories, Purdue University, Indiana (USA). The system under investigation was equipped with a variable-speed compressor and variable-speed fans, thus allowing the unit to meet different loads. A detailed mapping of the performance of this system was carried out by considering the effect of the outdoor temperature and the cooling load. In addition, the effect of evaporator fouling was investigated. Results showed that poor exergy performance were achieved due to the exergy destruction occurring in the evaporator. Also, when testing evaporator fouling, results showed that this fault contributed to increase the consumption of the mechanical exergy of the air, thus allowing for an easy detection of this fault.

1. Introduction

The increase in the global energy demand has been pushing research towards the exploitation of renewable energy sources and towards a more rational use of energy. To this aim, due to high energy consumption in air conditioning applications, an optimal design and operation of HVAC systems could lead to cost-effective energy savings and environmental benefits. Among HVAC systems, packaged rooftop unit (RTU) are widely used for air conditioning in commercial application. In order to improve the energy performance of these systems, more sophisticated control logics have been implemented, as the variable speed on compressor and fans which allows also for a better control of the indoor comfort conditions. Another important aspect is the energy consumption during the operation of these systems, which generally increases over time due to poor maintenance [1]. To this aim, some fault detection and diagnosis techniques (FDD) have been proposed and investigated in the literature [2],[3] and [4]. Among them, Thermoeconomic diagnosis is an innovative exergy-based FDD for detecting “faults” in energy systems [4]. This technique has been proven to be promising but still efforts are needed to improve its performance [5][6][7] [8] . To this aim, preliminary details into the exergy behavior of each component and the effects of the control system on the thermoeconomic model adopted are necessary [9].

This works aims at mapping the exergy performance of a packaged rooftop unit equipped with a variable-speed compressor and variable-speed fans by means of experimental data collected from a real unit. The performance of the system was evaluated by considering: (i) two values of outdoor temperatures and (ii) four levels of the RTU cooling capacity. The analysis was carried out on the basis of an ad-hoc thermoeconomic model, which is duly presented in this paper. After mapping the performance of the unit in the fault-free scenario, two levels of evaporator fouling were investigated. Assessment and comparison of the main exergy performance indicators for the fault-free and the faulty scenario will be presented.

2. Experimental set-up and testing procedures

A rooftop unit (RTU) was considered in this study having a rated capacity of 17.5 kW (5 ton) and a SEER rating of 20.0 (figure 1). The unit is equipped with a scroll compressor and a thermal expansion valve (TXV). The refrigerant used is R410a. The unit can be operated in a two-staged mode or in a variable speed mode. In a variable speed mode, both the compressor and the indoor fan speed are controlled in order to satisfy different cooling loads and avoiding the cycling of the unit. More specifically, the compressor speed is varied according to the supply air temperature setpoint (SAT_{sp}). Conversely, the indoor fan speed is controlled in order to meet the temperature setpoint for the indoor environment. A schematic of the test facilities is shown in figure 2. Two psychrometric chambers (each one equipped with its own reconditioning system) allowed to simulate the outdoor and indoor environment. A summary of the instrumentation installed on the RTU is presented in table 1. A real-time controller from National Instruments was used for data acquisition and control of the RTU.

Figure 1. Packaged rooftop air conditioning unit installed at Herrick Laboratories

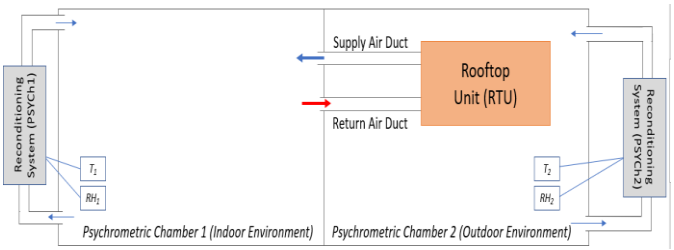

Figure 2. Packaged rooftop air conditioning unit installed at Herrick Laboratories

Table 1. Description of RTU instrumentation

	Sensors Type	**Sensors Location**
Refrigerant Temperature	*T-type Thermocouples* (Accuracy ±0.5°C)	Compressor Suction Compressor Discharge Condenser Outlet TXV inlet Evaporator Inlet Evaporator Outlet
Refrigerant Pressure	Pressure Transducers with voltage output (Accuracy ±0.5% of the full-scale reading)	Compressor Suction Compressor Discharge Liquid line outlet
Refrigerant Mass flowrate	*Coriolis Mass flowmeter* (Accuracy ±0.5% of the full-scale reading)	On the liquid line
Dry Bulb Air Temperature	*T-type Thermocouples (*Accuracy ±0.5°C*)*	Return Air: two-by-two grid was spaced equally in a rectangular grid placed before the evaporator Supply Air: two-by-two grid spaced equally in a rectangular grid placed after the supply fan Condenser Inlet: 8 thermocouples mounted in a four-by-two grid on the face of the condenser Condenser Outlet: 4 thermocouples mounted radially on the condenser outlet

Dew Point Air Temperature	*Dew point hygrometer with chilled mirror probe* (Accuracy ±0.15°C)	Air samples were taken before the evaporator inlet and at the beginning of the supply air duct
Power Consumption	*Watt Transducers* (Accuracy of ±0.5 % of the full-scale reading)	Indoor Fan Supply Air Compressor Power Condenser Fan

2.1. Description of testing procedures

In order to evaluate the performance of the unit at different load level, a set of different air mass flowrate across the evaporator were tested by varying the indoor fan torque. More specifically, the torque was varied from 100% of its maximum value (in this case, the unit provides the maximum cooling capacity) down to 30% (minimum RTU cooling capacity) while keeping the supply air temperature setpoint (SAT_{sp}) equal to 15°C. For all tested conditions, the temperature and relative humidity of the air returning to the unit from the indoor environment were kept constant and equal to 26.5°C and 50%.

As concerns the effect of the boundary conditions, two values of the outdoor temperature (here indicated as Toutdoor) were investigated: 30°C and 35°C. The operation of the unit at each set of driving conditions was first recorded with no faults imposed. Then, the evaporator fouling was introduced and all tests were repeated. Measurements were taken every second for all of the input and output variables. The steady state of the system was detected by comparing data of a moving averaging window of 20 minutes.

Evaporator fouling was tested by acting on the opening of an iris damper placed on the supply air duct of the unit. Different levels were selected by measuring the air pressure drop across the RTU while running the indoor fan at its maximum speed (around 1250 rpm). Considering a 150 Pa air pressure drop (about 0.6 inch of water) across the RTU for the fault-free scenario (i.e. when the damper is fully open), two levels of fouling were tested: (i) a "light" fault which corresponds to a 280 Pa air pressure drop (about 1.0 inch of water) and (ii) a "heavy" evaporator fouling which corresponds to 380 Pa air pressure drop (about 1.5 inches of water).

3. Exergy analysis and thermoeconomic modelling of the examined system

Exergy analysis of the examined system was carried out on the basis of the thermoeconomic model adopted for this system. More specifically, in Thermoeconomics exergy flows entering and exiting a given component are defined on the basis of its *productive scope* [7]. For instance, an evaporator coil for cooling and dehumidifying an air stream aims at increasing the thermal and chemical exergy of the air (which is then identified as its productive scope) by exploiting the thermal and mechanical exergy of the refrigerant. The exergy flow produced is generally identified as a "Product", and the amount of exergy used to this aim is usually identified as "Fuel". Due to the need to identify a productive scope for components, exergy flow related to a stream of matter (for instance, refrigerant and air in cooling application) is splitted into its "thermal", "mechanical" and chemical" fractions, which are respectively related to the temperature, pressure and composition disequilibria between its thermodynamic state and the ambient dead state. The procedures followed for calculating these fractions are here omitted, thus details can be found in [10]. In figure 3, the thermoeconomic model of the investigated RTU is presented.

It is worth observing that:

1. The compressor increases both the thermal and the mechanical exergy of the refrigerant, i.e. $\Delta\dot{B}_1^{\mathrm{T}}$ and $\Delta\dot{B}_1^{\mathrm{M}}$ by using a mechanical exergy flow provided by an electric motor. In this case, since both the compressor and the electric motor were treated as a unique component, the electric power is the exergy flow directly consumed by the compressor.
2. The condenser aims at discharging the thermal exergy content of the refrigerant, i.e. $\left|\Delta\dot{B}_2^{\mathrm{T}}\right|$ into an air flowrate coming from the outdoor environment, by consuming: (i) the electric power to drive the fan, i.e. $\dot{W}_{e,2}$ (in this case the condenser and its fan are considered as a unique

component) and (ii) the mechanical exergy of the refrigerant $\left|\Delta \dot{B}_2^{\mathrm{M}}\right|$ due to pressure losses on refrigerant side.

3. The thermal expansion valve uses the mechanical exergy flow $\left|\Delta \dot{B}_3^{\mathrm{M}}\right|$ produced by the compressor to increase the thermal exergy of the refrigerant (i.e. $\Delta \dot{B}_3^{\mathrm{T}}$), then supplied to the evaporator.
4. The evaporator increases the thermal and chemical exergy of the air by means of the following exergy flows: (i) the mechanical exergy $\left|\Delta \dot{B}_4^{\mathrm{M}}\right|$ of the refrigerant dissipated by the pressure drop on the refrigerant side, (ii) the thermal exergy of the refrigerant $\left|\Delta \dot{B}_4^{\mathrm{T}}\right|$ and (iii) the mechanical exergy of the air $\left|\Delta \dot{B}_{\mathrm{air}}^{\mathrm{M}}\right|$ which is dissipated by pressure drop on air side.
5. the indoor fan increases the mechanical exergy of the air in order to balance the pressure drop across the evaporator, by using the mechanical power provided by an electric motor. Here, both the indoor fan and its electric motor are considered as a unique component, thus the electric power is the exergy flow consumed by this component.

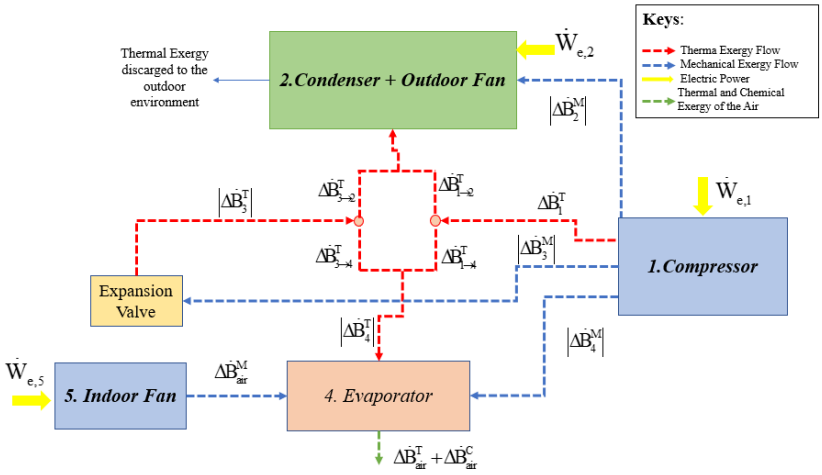

Figure 3. Thermoeconomic model of the rooftop unit

In order to assess the exergy performance of each component, the *unit exergy consumption of the i-th component* k_i was used in this work. This indicator is the ratio between the exergy used by the i-th component (here indicated as F_i) to produce the unit exergy of its product P_i, i.e. $k_i = F_i / P_i$. For instance, the unit exergy consumption of the evaporator k_4, here shown in equation 1, is the ratio between the following exergy quantities: (i) the reduction in the thermal and mechanical exergy of refrigerant plus the mechanical exergy of the air and (ii) the increase in thermal and chemical exergy of the air cooled and dehumidified across the evaporator.

$$k_4 = \frac{\left|\Delta B_4^{\mathrm{T}}\right| + \left|\Delta B_4^{\mathrm{M}}\right| + \Delta B_{\mathrm{air}}^{\mathrm{M}}}{\Delta B_{\mathrm{air}}^{\mathrm{C}} + \Delta B_{\mathrm{air}}^{\mathrm{T}}} \tag{1}$$

In order to quantify the percentage of the exergy destroyed in the thermostatic valve, the quantity χ_3 was defined as in equation 2. Particularly, ΔB_3^{T} is the increase in the thermal exergy of the refrigerant across the valve and $\left|\Delta B_3^{\mathrm{M}}\right|$ is the mechanical exergy of refrigerant consumed to this aim.

$$\chi_3 = \frac{\Delta B_3^{\mathrm{T}}}{\left|\Delta B_3^{\mathrm{M}}\right|} \tag{2}$$

4. Results and discussion

In this section, the following results are shown: (i) energy and exergy performance of the RTU in the free-fault scenario (ii) energy and exergy performance of the unit when evaporator fouling is imposed.

4.1. Energy and Exergy Performance in the fault-free scenario

In table 2, thermodynamic data measured during the experimental activities are shown. Only results for $T_{outdoor}$= 30°C are shown, being the same trends verified for $T_{outdoor}$=35°C. The indoor fan torque was set equal to 100%, 80%, 50% and 30%. The minimum cooling capacity, i.e. 10.3 kW, is achieved by setting the fan torque to 30%, and it is equal to the 55% of the maximum cooling capacity (i.e. 18.7 kW). Also, as concerns the sensible load fraction of the cooling capacity, here expressed by the sensible to heat ratio values SHR (which is the ratio between the sensible load and the cooling load), it is approximately constant for all load levels considered. Condensing pressure decreases when reducing the cooling capacity, conversely, the evaporating pressure is approximately constant. The supply dry bulb temperature is approximately equal to the setpoint (i.e. 15°C) and the electrical power consumed by the compressor decreases as the control system reduced the compressor speed.

Table 2. Thermodynamic Data measured for the following test conditions: T_{indoor}=26.5°C, RH= 50% $T_{outdoor}$=30°C and SAT_{sp}= 15°C

Indoor Fan Torque Percentage	***Air Mass Flowrate***	***Return Air***		***Supply Air***		***Indoor Fan Power***	***Outdoor Fan Power***	***Sensible Capacity***	***Cooling Capacity***	***SHR***
		Dry Bulb Temp.	*Dew Point Temp.*	*Dry Bulb Temp.*	*Dew Point Temp.*					
	[kg/s]	[°C]	[°C]	[°C]	[°C]	[W]	[W]	[W]	[W]	[W/W]
100%	1.273	26.5	11.98	12.07	15.20	1125	293	14700	18774	0.783
80%	1.157	26.5	12.21	11.97	14.80	809	292	14189	18322	0.774
50%	0.901	26.5	12.20	12.05	14.78	389	216	11013	14394	0.765
30%	0.678	26.5	12.30	12.26	14.90	173	162	8102	10362	0.782

Indoor Fan Torque Percentage	***Refrigerant Quality***	***Suction Pressure***	***Suction Temp.***	***Suction Superheat***	***Discharge Pressure***	***Subcooling***	***Refrigerant Mass Flowrate***	***Compressor Power***
	[-]	[kPa]	[°C]	[°C]	[kPa]	[°C]	[kg/s]	[W]
100%	0.16	1087.6	15.2	5.76	2500.1	8.93	0.101	3323
80%	0.16	1073.1	14.4	5.56	2495.9	8.82	0.099	3253
50%	0.17	1083.8	15.7	5.20	2387.6	8.11	0.089	2334
30%	0.17	1099.3	14.9	4.91	2283.8	6.59	0.066	1594

In figure 3, the energy efficiency ratio (EER) values, which is the ratio between the RTU cooling capacity and the sum of electrical consumption of the indoor fan, outdoor fan and the compressor, are shown for the two tested outdoor temperatures (i.e. 30°C and 35°C) and for different RTU cooling capacities. Regardless the temperature of the outdoor environment, the EER increases when reducing the cooling capacity of the unit due to the reduction in the condensing pressure. Also, for a fixed cooling capacity, a reduction of the EER is observed when increasing the outdoor temperature.

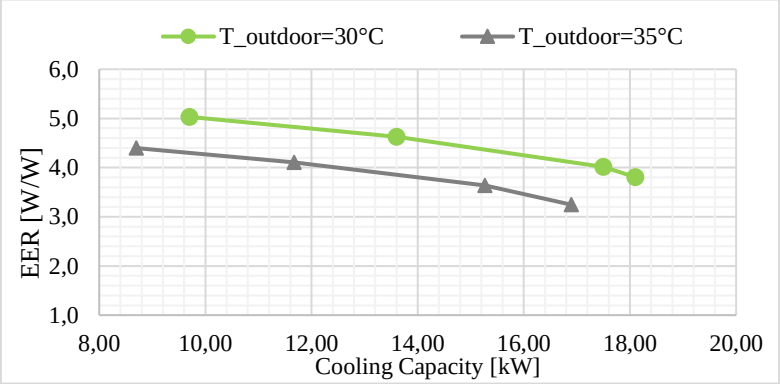

Figure 3. Energy Efficiency Ratio (EER) values for the fault-free scenario

In table 3, exergy results are presented on the basis of the model shown Figure 1. This analysis was carried out by means of Engineering Equation Solver [11]. It is worth observing that:

- the unit exergy consumption of the compressor (i.e. k_1) slightly increases when the capacity of the unit is reduced. This trend is related to the isoentropic efficiency of the compressor, which decreases in the examined range.
- regardless the considered cooling capacity, the mechanical exergy produced by the compressor is largely used by the TXV, being negligible the ones consumed respectively by the evaporator and the condenser. Also, both the mechanical and the thermal exergy provided by the compressor decreases when reducing the cooling capacity due to reduction in the refrigerant mass flowrate and in the pressure ratio.
- the percentage of exergy destruction in the TXV is approximately constant for all load level.
- high values of the evaporator unit exergy consumption (i.e. k_4) are observed.
- the mechanical exergy of the air decreases when reducing the RTU capacity, due to decreasing in both air mass flowrate and pressure drop across the evaporator. Also, the unit exergy consumption of the indoor fan is not sensitive to the load level.

Table 3. Exergy flows for each component for the following test conditions: T_{indoor}=26.5°C, RH= 50% $T_{outdoor}$=30°C and SAT_{sp}= 15°C

			Indoor Fan Torque Percentage			
			100%	**80%**	**50%**	**30%**
1.Compressor	$\dot{W}_{e,1}$	[kW_{ex}]	3.323	3.253	2.334	1.594
	ΔB_1^T	[kW_{ex}]	0.782	0.746	0.496	0.281
	ΔB_1^M	[kW_{ex}]	1.650	1.611	1.194	0.836
	k_1	[kW_{ex}/ kW_{ex}]	1.366	1.380	1.381	1.428
2. Condenser	$\dot{W}_{e,2}$	[kW_{ex}]	0.293	0.292	0.216	0.162
	$\lvert\Delta B_2^T\rvert$	[kW_{ex}]	0.82	0.83	0.72	0.58
	$\lvert\Delta B_2^M\rvert$	[kW_{ex}]	0.012	0.010	0.005	0.003
3.TXV	ΔB_3^T	[kW_{ex}]	1.391	1.357	1.011	0.709
	$\lvert\Delta B_3^M\rvert$	[kW_{ex}]	1.636	1.598	1.188	0.832
	χ_3	[kW_{ex}/ kW_{ex}]	0.150	0.149	0.151	0.152

	$\left\|\Delta B_4^{\mathrm{T}}\right\|$	[kW_{ex}]	1.346	1.374	1.354	1.306
	$\left\|\Delta B_4^{\mathrm{M}}\right\|$	[kW_{ex}]	0.010	0.009	0.011	0.012
4.Evaporator	$\left\|\Delta B_{\mathrm{air}}^{\mathrm{T}}\right\|$	[kW_{ex}]	0.443	0.427	0.329	0.242
	$\left\|\Delta B_{\mathrm{air}}^{\mathrm{C}}\right\|$	[kW_{ex}]	0.069	0.071	0.057	0.036
	k_4	[kW_{ex}/ kW_{ex}]	4.836	4.236	3.545	3.085
	$\dot{W}_{\mathrm{e},5}$	[kW_{ex}]	1.12	0.81	0.39	0.17
5. Indoor Fan	$\left\|\Delta B_{\mathrm{air}}^{\mathrm{M}}\right\|$	[kW_{ex}]	0.221	0.153	0.060	0.030
	k_{fan}	[kW_{ex}/ kW_{ex}]	5.07	5.27	6.45	5.79

The overall exergy performance is calculated according to equation 3.

$$\eta_{\mathrm{ex,RTU}} = \frac{\Delta\dot{B}_{\mathrm{air}}^{\mathrm{C}} + \Delta\dot{B}_{\mathrm{air}}^{\mathrm{T}}}{\dot{W}_{e,1} + \dot{W}_{e,5} + \dot{W}_{e,2}} \tag{3}$$

Results for $\eta_{\mathrm{ex,RTU}}$ are shown in figure 4. The overall exergy performance is very poor (i.e. under 15%). Most of the exergy destruction is located in the evaporator as testified by the values of k_4 in Table 3. The exergy performance of the RTU increases when the cooling capacity is reduced and when lower outdoor temperatures are considered.

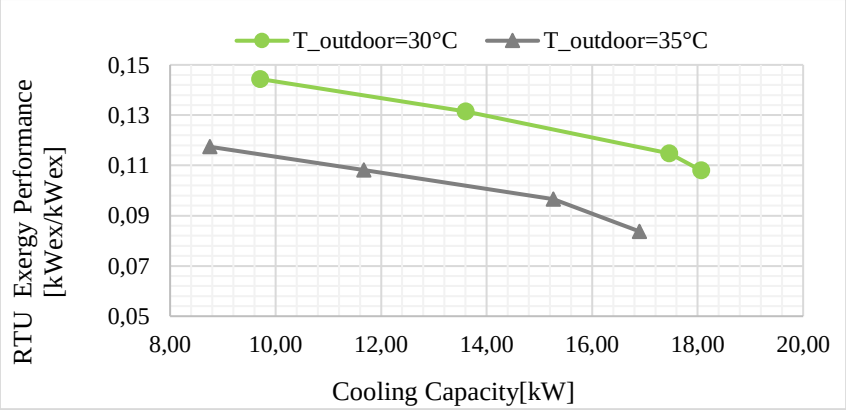

Figure 4. RTU exergy performance for different outdoor temperatures and different cooling capacity in the fault free scenario

4.2 Effect of evaporator fouling on the energy and exergy performance of the RTU.
Experimental results for the evaporator fouling are shown in figure 5. First of all, the main effect of this fault is the reduction in the air mass flowrate across the evaporator. When running the indoor fan at its maximum speed (i.e. 1250 rpm), the following percentage reductions in air mass flowrate were observed: (i) 10% for the light fouling scenario and (ii) 25% for the heavy one. In figure 5, the sensible capacity is shown on the x-axis instead of the total cooling capacity. In fact, since the unit is controlled on the basis of temperature measurement, it is reasonable to compare fault-free and faulty scenarios where the RTU provides the same sensible cooling capacity. It is worth noting that:

1. when the indoor fan is running at the maximum speed, only 12 kW of sensible capacity are provided with respect to 14.5 kW for a fault-free scenario.
2. a slight decrease in both condensing and evaporating pressure is observed;
3. for a fixed sensible capacity, the power consumed by the compressor increases due to the higher refrigerant mass flowrate.
4. a decrease in the EER values is observed. For instance, considering the maximum sensible capacity provided in the heavy fouling scenario, i.e. 12 kW, an EER=3.8 W/W is achieved with respect to 4.2 W/W in the fault-free one.

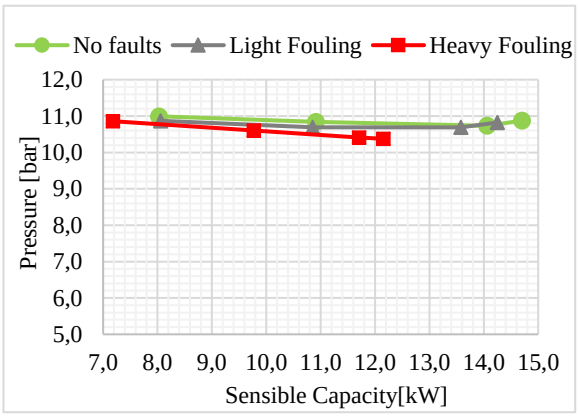

(a)

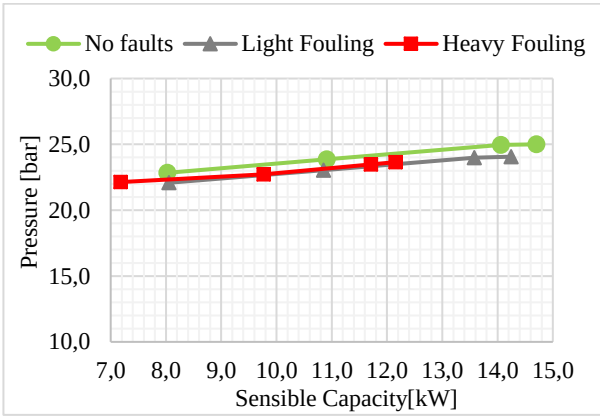

(b)

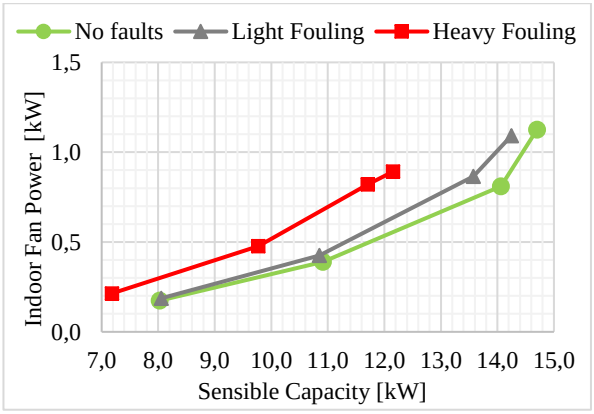

(c)

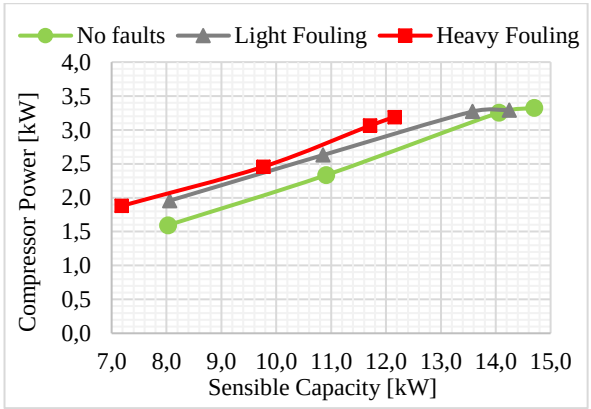

(d)

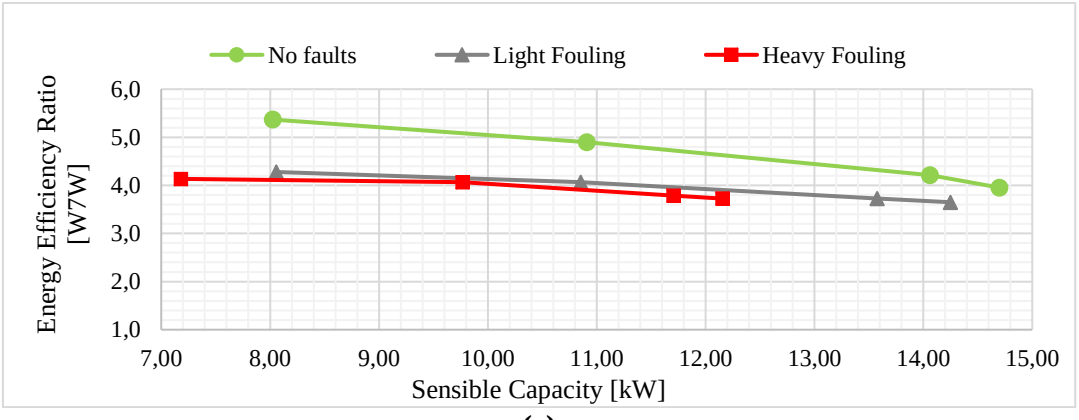

(e)

Figure 5: Thermodynamic results for evaporator fouling: **(a)** evaporating pressure **(b)** condensing pressure **(c)** indoor fan power **(d)** compressor power **(e)** EER values

For a sake of clarity, in Figure 6 only results for $T_{outdoor}$=30°C are shown. The same trends are observed for $T_{outdoor}$=35°C. The unit exergy consumption of the compressor, i.e. $k_{1,}$ is plotted in Figure 6a. Results showed that for a fixed sensible load, the compressor unit exergy consumption is approximately constant regardless the level of fault imposed. The exergy destruction percentage in the TXV, i.e. χ_3 in Figure 6b show also that for a fixed sensible constant value regardless the level of fault imposed on the evaporator.

Results for the evaporator exergy unit consumption are shown in Figure 6c and 6d. More specifically, the consumption of air mechanical exergy per unit exergy product of the evaporator, i.e. $k_{4,5}$ increases when passing from a fault-free to a faulty scenario due to the increased air pressure drop across the evaporator. Conversely, the unit exergy consumption of refrigerant thermal exergy, i.e. $k_{4,ref}$ is not sensitive to the fault level. These results suggest that detection of evaporator fouling can be easily achieved only by checking variation in the $k_{4,5}$ values

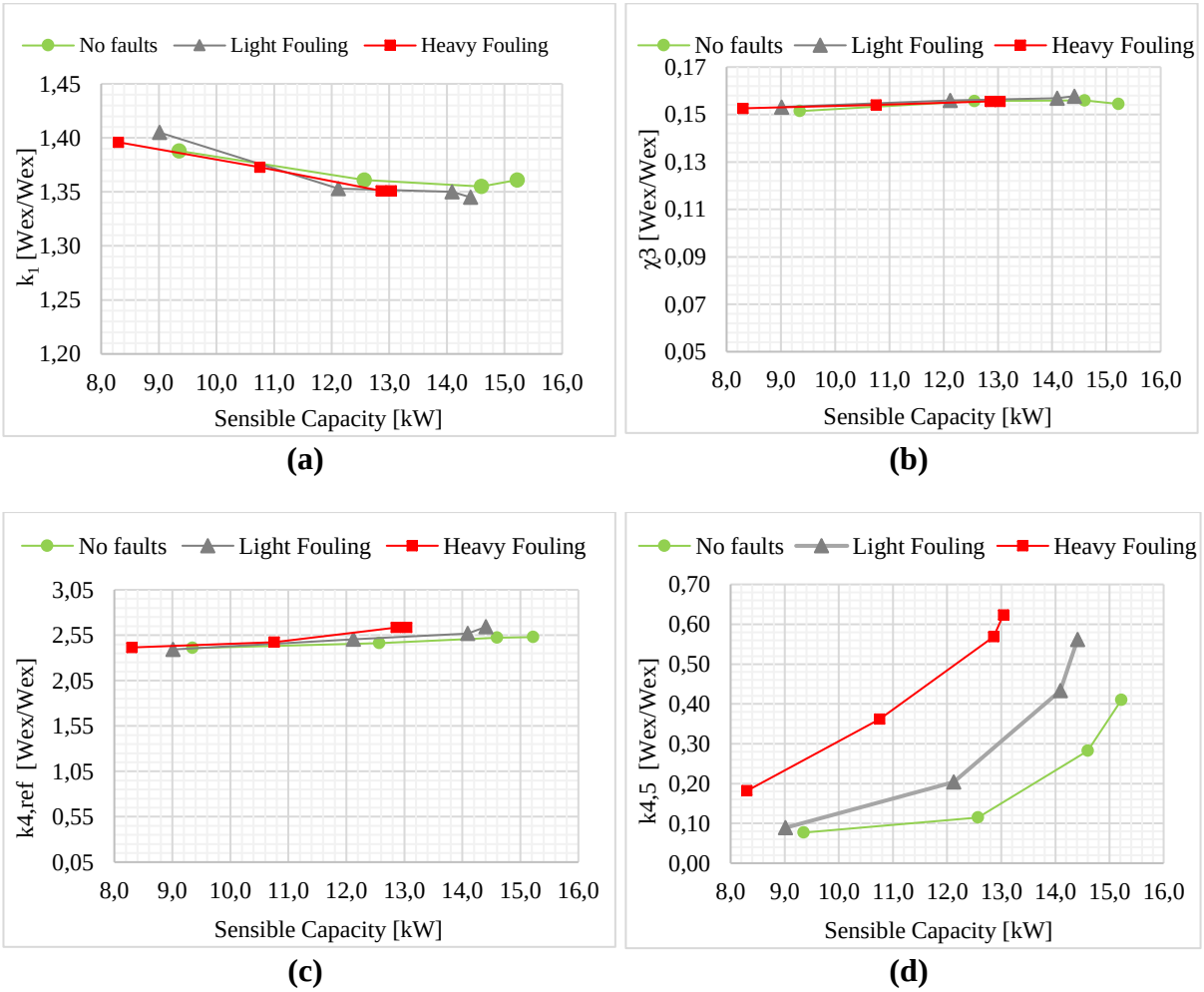

Figure 6: (a) Unit exergy consumption of the compressor k_1 **(b)** exergy destruction percentage χ_3 in TXV **(c)** evaporator unit exergy consumption of refrigerant thermal exergy **(d)** unit exergy consumption of mechanical exergy of the air in the evaporator

5. Conclusion

This work aims at mapping the exergy performance of a packaged air conditioning unit equipped with a variable speed-fans and variable speed-compressor. The results showed that energy performance ratio of the unit increases when the cooling load decreases as a consequence of the lower pressure ratios. The overall exergy performance of the unit is poor mainly due to exergy destruction occurring at the evaporator. Some improvements were observed when the RTU capacity is reduced. When investigating evaporator fouling, results suggested that the fault affected mainly consumption of the mechanical air exergy, thus allowing for an easy detection of the fault

References

[1] Breuker M G and Braun J E 1998 Common Faults and Their Impacts for Rooftop Air Conditioners *HVAC&R Research* **4** 303-18

[2] Rossi T M and Braun J E 1997 A statistical rule-based fault detection and diagnostic method for vapor compression air conditioners *HVAC&R Research* **3** 19-37

[3] Li H and Braun J E 2007 Decoupling features and virtual sensors for diagnosis of faults in vapor compression air conditioners *Int. J. Refrigeration* **30** 546–64

[4] Uson S and Valero A 2010 Thermoeconomic Diagnosis of Energy Systems*, Prensa Universidad de Zaragoza* Zaragoza Spain.

[5] Piacentino A. and Talamo M 2013 Innovative thermoeconomic diagnosis of multiple faults in air conditioning units: methodological improvements and increased reliability of results, *Int. J. Refrigeration* **36** 2343-65

[6] Torres C, Valero A, Serra L, Royo J 2002 Structural theory and thermoeconomic diagnosis: Part I. On malfunction and dysfunction analysis *Energy Conversion and Management* **43** 1503-18.

[7] Torres C 2004 Symbolic thermoeconomic analysis of energy systems. In: Frangopoulos CA, editor. *Exergy, energy system analysis and optimization, from encyclopedia of life support system (EOLSS)*. Oxford: EOLSS Publishers. Available at: (hhttp://www.eolss.net).

[8] Valero A, Correas L, Zaleta A, Lazzaretto A, Verda V, Reini M, Rangel V, 2004 On the thermoeconomic approach to the diagnosis of energy system malfunctions: Part 2. Malfunction definitions and assessment. *Energy*, **29** 1889-1907

[9] Verda V 2006 Accuracy level in thermoeconomic diagnosis of energy systems *Energy* **31** 3248-260

[10] Szargut J 2005 Exergy Method: Technical and Ecological Applications *WITpress*

[11] Klein S.A. 2010 Engineering equation solver V9.810. Middleton, WI: Solar Energy Laboratory, *F-Chart Software*